Journal of Alloys and Compounds 512 (2012) 94–99

Contents lists available at SciVerse ScienceDirect

Journal of Alloys and Compounds

journal homepage: www.elsevier.com/locate/jallcom

Structure, magnetic, and magnetocaloric properties of amorphous and crystalline $La_{0.4}Ca_{0.6}MnO_{3+\delta}$ nanoparticles

Paula Lampen, Archana Puri, Manh-Huong Phan*, Hariharan Srikanth**

Department of Physics, University of South Florida, USA

ARTICLE INFO

Article history:
Received 13 August 2011
Received in revised form 7 September 2011
Accepted 8 September 2011
Available online 22 September 2011

PACS:
75.30.Sg

Keywords:
Amorphous and nanocrystalline manganites
Magnetic properties
Magnetocaloric effect
Magnetic refrigeration

ABSTRACT

We report a systematic study of the effects of size reduction on the magnetic and magnetocaloric properties of amorphous and crystalline $La_{0.4}Ca_{0.6}MnO_{3+\delta}$ nanoparticles. The materials were synthesized using a modified wet chemical Pechini route, starting with nitrate precursors to produce the perovskite structure. Phase purity, structure, size, and crystallinity were investigated using XRD and TEM. Thermal treatments resulted in nanocrystals with average diameters of 25 nm, 50 nm, and 130 nm, as well as amorphous particles ~10 nm in diameter. Magnetic measurements revealed broad, second order ferromagnetic transitions in the nanocrystals. As particle size increased from 10 nm to 130 nm, the Curie temperature shifted from 40 K to 255 K. Magnetization, magnetic entropy change (ΔS_M), and refrigerant capacity (*RC*) also increased with size in the nanocrystalline samples. For a field change of 5 T, the 130 nm particles exhibit a magnetic entropy change of 2.8 J/kg K and a large refrigerant capacity of ~240 J/kg at 250 K. Interestingly, the 10 nm amorphous particles undergo the sharpest magnetic transition, leading to a larger value of ΔS_M than in the 25 nm or 50 nm crystalline particles. These results reveal that size reduction has a significant impact on the magnetic and magnetocaloric properties of $La_{0.4}Ca_{0.6}MnO_{3+\delta}$.

1. Introduction

In recent years, magnetic refrigeration based on the magnetocaloric effect (MCE) has emerged as a promising alternative to the less efficient gas compression cycle methods [1–3]. However, the need for improved performance in magnetocaloric materials at moderate fields and over a large temperature interval remains an obstacle to the wide-scale adoption of magnetic refrigeration technology. Perovskite structured manganese oxides have been demonstrated to be effective MCE materials, generating great interest due to their cost-effectiveness, tunability, and ease of preparation (see the review paper by Phan et al.) [2]. The MCE refers to the change in temperature that accompanies the adiabatic application of a magnetic field to a system of disordered spins, caused by the lattice entropy increasing to compensate the decrease in magnetic entropy (ΔS_M). This effect is pronounced in mixed valence manganites of the form $R_{1-x}M_xMnO_3$ (R = La, Pr, Nd, Sm and M = Sr, Ca, Ba, Pb), in which the variation of the double exchange interaction of the Mn^{3+} and Mn^{4+} ions leads to large entropy changes [2]. While high values of ΔS_M are desirable, a more important figure of merit for an effective magnetic refrigeration material is the refrigerant capacity or relative cooling power (*RC*). *RC* is a measure of heat transfer between the cold and hot sinks in an ideal refrigeration cycle and depends on both the magnitude and full width at half maximum of the ΔS_M peak. Materials undergoing a first order magnetic transition often exhibit large ΔS_M peaks over a narrow temperature range, while second order transitions tend to show smaller ΔS_M values over a wider range of temperatures. The broader nature of the second order transition can lead to enhanced *RC* values when compared with first order transitions after subtracting hysteretic losses [4]. Reducing the size of a material to the nanoscale has been found to broaden or change the order of a transition from first to second [5–7]. For this reason, nanoparticles of manganites have been found to be effective MCE materials [6–11].

Manganite nanoparticles have been successfully synthesized by many methods including co-precipitation [12], glycine–nitrate [13], combustion [14], hydrothermal decomposition [15], spray pyrolysis [10], and sol–gel [5,7,9,11]. Sol–gel is the most widely used technique due to its low cost, versatility, low-temperature processing, and homogeneous products [16]. In particular, the Pechini method of sol–gel processing forms stable complexes with a large variety of metals over a wide pH range, allowing for relatively simple synthesis of oxides of considerable complexity [17]. The Pechini method uses a mixture of metal salts as precursors, citric acid (CA) as chelating ligands of metal ions and polyethylene glycol (PEG) as a cross linking agent to form a polymeric resin on a molecular level. Upon heating, CA and PEG polymerize to

* Corresponding author. Tel.: +813 974 47 14.
** Corresponding author.
E-mail addresses: phanm@usf.edu (M.-H. Phan), sharihar@usf.edu (H. Srikanth).

0925-8388/$ – see front matter © 2011 Elsevier B.V. All rights reserved.
doi:10.1016/j.jallcom.2011.09.027

form an organic network, in which cations are immobilized and distributed homogeneously on the molecular scale [18]. The segregation of particular metal ions is reduced and compositional homogeneity of fine powders with high surface area can be attained at low calcination temperatures, resulting in particles with small size and phase purity. In this study, we examine the effects of particle size on the magnetic and magnetocaloric properties of $La_{0.4}Ca_{0.6}MnO_3$ nanoparticles prepared by the Pechini method.

2. Experimental details

The starting solution was prepared from metal nitrates (MN), citric acid (CA), and polyethylene glycol (PEG). Aqueous metal nitrate solutions with 0.5 molarity were prepared by dissolving $(LaNO_3)_2{\cdot}6H_2O$, $Ca(NO_3)_3{\cdot}6H_2O$, and $Mn(NO_3)_3{\cdot}xH_2O$ in deionized water. The solutions were mixed together in stochiometric ratios, and CA was added with the molar ratio of MN:CA = 1:3 to form stable citrate–metal ion complexes. After heating the solution to 80 °C for 1hr with stirring, PEG was added. PEG serves as a cross-linking agent between the metal complexes, allowing polymerization to occur. The solution was placed under vacuum and heating was adjusted to maintain a constant vapor temperature of 80 °C as the solvents evaporated. A dense, translucent polymer resin was formed as an intermediate stage, which solidified upon further heating under vacuum. After grinding with an agate mortar, the resulting black powder was treated at 500 °C for 3 h to remove the organic materials. The powder was divided and calcined separately at 700 °C for 3 h, 850 °C for 3 h, and 1000 °C for 7 h in air. A 5 °C/min ramping rate was used during all heating and cooling processes. X-ray diffraction was carried out with the Bruker D8 Focus X-ray diffractometer operating with Cu-Kα radiation (λ = 1.5406 Å). The magnetic and magnetocaloric properties were measured using a commercial Quantum Design Physical Property Measurement System (PPMS) with a vibrating sample magnetometer over a temperature range of 10–320 K and fields up to 5 T. The temperature dependence of magnetization was investigated using a field of 200 Oe. While acquiring the low temperature M–H loops, a sweep rate of 30 Oe/s was used in the small-field range to determine coercivity. Magnetization isotherms were measured from 0 to 5 T with a field step of 100 Oe and a temperature interval of 5 K in the amorphous samples and 10 K in the nanocrystals.

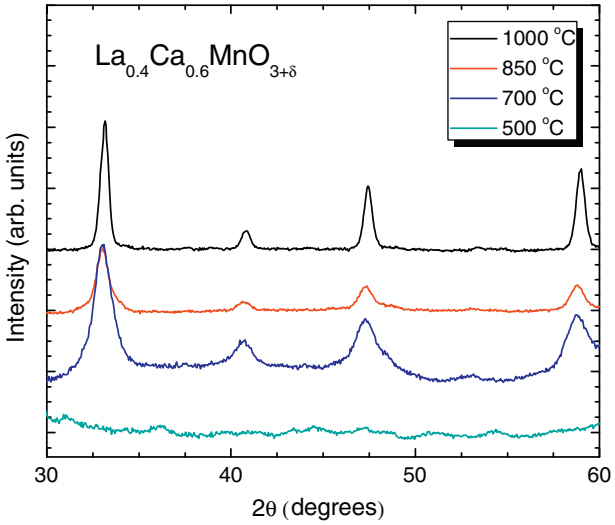

Fig. 1. Room temperature X-ray diffraction pattern for the $La_{0.4}Ca_{0.6}MnO_3$ nanoparticles annealed at various temperatures.

3. Results and discussion

Fig. 1 shows the room temperature XRD patterns for each sample. The scans demonstrate the absence of impurity phases. In agreement with the literature, all samples correspond to the *Pnma* space group and orthorhombic structure [12,19,20] with lattice parameters of $a = 5.403$, $b = 7.613$ and $c = 5.412$ Å. The absence of well-defined peaks in the sample calcined only at 500 °C indicates that the particles are mainly amorphous in nature, while heat treatments above 500 °C yielded crystalline particles. TEM images

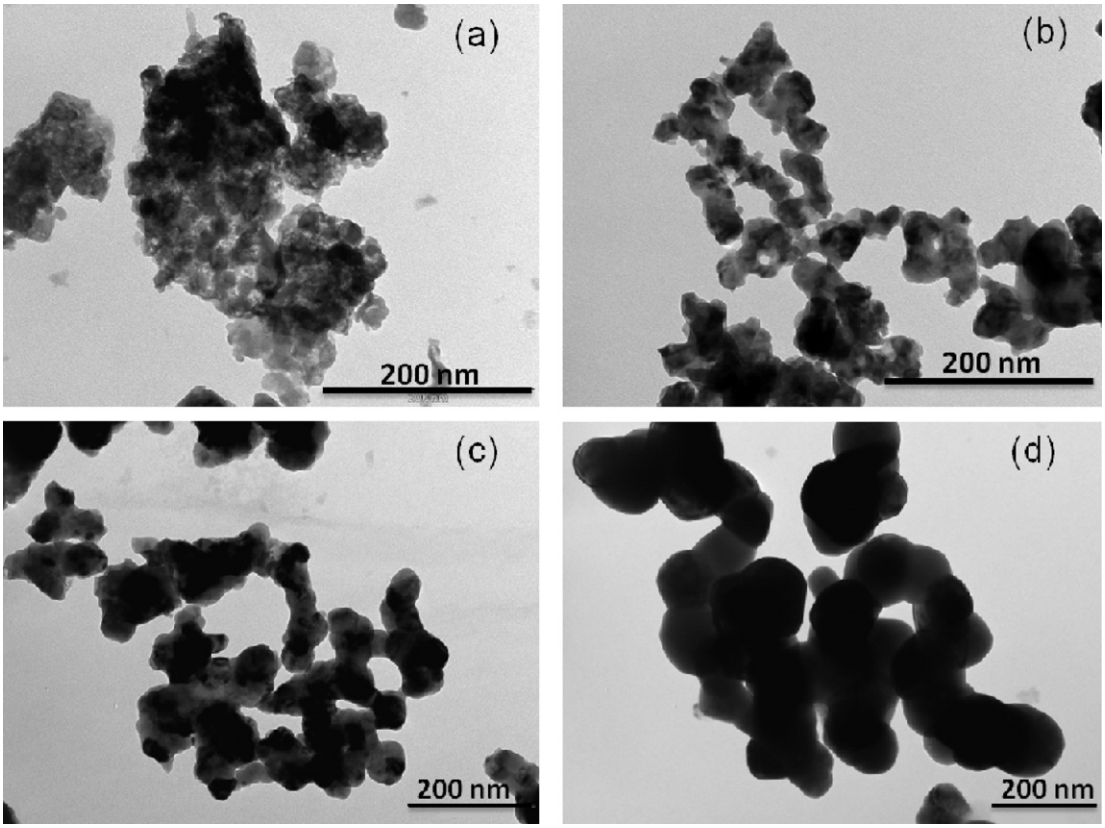

Fig. 2. TEM micrographs of nanoparticles obtained after calcinations at (a) 500 °C, (b) 700 °C, (c) 850 °C, and (d) 1000 °C. Average particle sizes were determined to be 10 nm, 25 nm, 50 nm, and 130 nm, respectively.

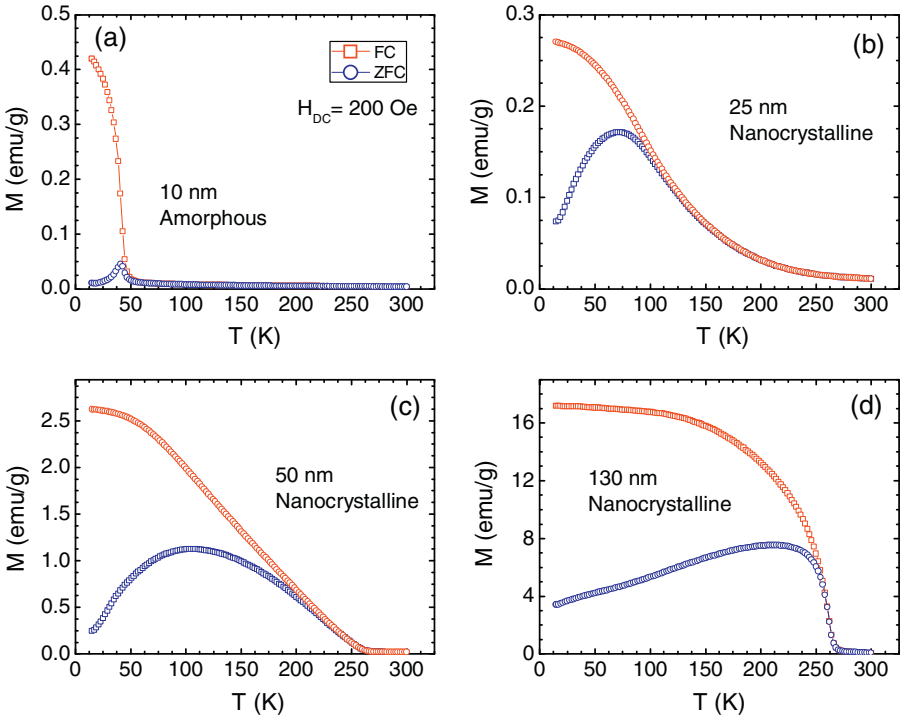

Fig. 3. Field-cooled and zero field-cooled temperature dependent magnetization curves of (a) 10 nm, (b) 25 nm, (c) 50 nm, and (d) 130 nm $La_{0.4}Ca_{0.6}MnO_3$ measured under a DC field of 200 Oe.

(Fig. 2) give average particle diameters of ~10 nm, 25 nm, 50 nm, and 130 nm, for the samples treated at 500 °C, 700 °C, 850 °C, and 1000 °C, respectively.

Fig. 3 shows the temperature dependence of the field-cooled (FC) and zero field-cooled (ZFC) magnetization of amorphous and nanocrystalline $La_{0.4}Ca_{0.6}MnO_{3+\delta}$. Consistent with the previous results for sol–gel synthesized $La_{0.4}Ca_{0.6}MnO_3$ nanocrystals [19,20], the samples in the present case exhibit only FM-like behavior, as can be seen from the smooth increase in the *M*–*T* curves without a low-*T* drop in magnetization that would indicate a stable CO phase. We also observe that magnetization decreases significantly with decreasing particle size; this trend is expected in FM nanoparticles as long-range ferromagnetic order is lost and surface spin disorder becomes increasingly significant [21]. On the other hand, a reduction of particle size in CO manganites will at first result in an increase in magnetization as long range CO strains are reduced and FM order is established at the particle surface [22]. This second trend was observed in the size-effects study by Liu et al. [20]. However, in the present case the monotonic dependence of magnetization on size suggests that either CO does not appear in any appreciable amount even in the largest particles, or it is weak enough to be aligned by a 200 Oe field, i.e. is short-range in nature. The discrepancy can be attributed to variation in the oxygen content, which can alter the relationship between the double- and superexchange interactions [23].

While CO does not play an overt role, other indicators point to a significant degree of disorder in the FM state. The large irreversibility between the FC and ZFC curves and the peak in the ZFC magnetization are typical features of a cluster glass material [24]. Inverse susceptibility versus temperature is plotted in Fig. 4. Fitting to the Curie–Weiss law shows an increase of the Curie temperature from 145 K to 250 K as particle size is increased from 25 nm to 130 nm. The downturn in χ^{-1} in the 130 nm and 50 nm samples is characteristic of the onset of a Griffiths-like phase, a well-known phenomenon in doped manganites [25–28]. Induced by disorder, the Griffiths phase features FM clusters within the PM phase between the Curie temperature of the undiluted system (T_G) and the actual magnetic ordering temperature ($T_C(p)$). The inset of Fig. 4 shows the inverse susceptibility of the 10 nm amorphous particles. Extrapolating a high-*T* fit to the temperature axis gives a negative intercept, likely due to a glassy behavior.

To assess the nature of magnetic phase transitions in the present compounds, Arrott plots of samples of each particle size are displayed in Fig. 5. According to the Banerjee criterion [29], the sign of the slope of H/M vs. M^2 is determined by the nature of a PM to FM transition, with a negative slope corresponding to a first order transition and a positive slope corresponding to a second order

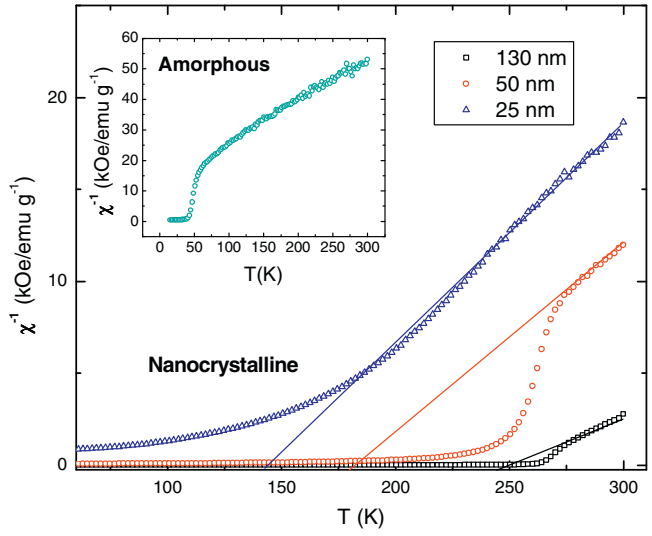

Fig. 4. Temperature dependent inverse susceptibility in the nanocrystalline particles. The lines represent fits of the high temperature data to the Curie–Weiss law to determine T_C. The inset shows the inverse susceptibility of the amorphous sample.

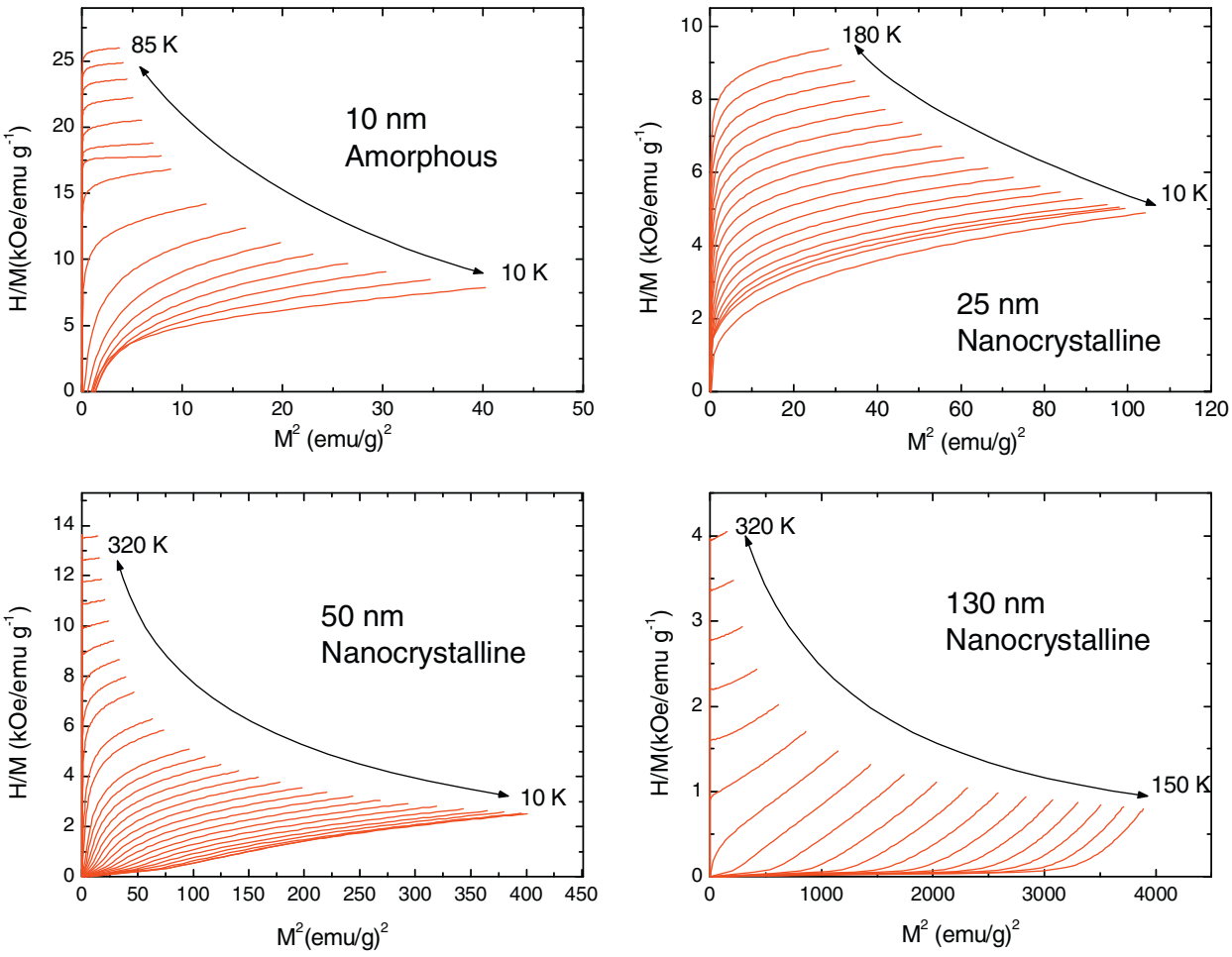

Fig. 5. Arrott plots for various temperatures around T_C for samples with each particle size.

transition. By this criterion, the 130 nm samples clearly undergo a second order transition. A simple mean field model of a long-range ferromagnet predicts that H/M should vary linearly with M^2. The deviation from the mean field model is most significant in the amorphous particles (Fig. 5). The H/M vs. M^2 isotherms show large curvature and do not change concavity below the transition, instead bunching together at lower temperatures. This behavior can be seen as a manifestation of short range ordering. Some clustering is also present in the 25 nm and, to a lesser extent, the 50 nm samples. Clearly, the magnetic ordering is affected by particle size. By increasing the calcination temperature and, consequently, particle size, we improve the magnetic and crystalline properties of the particles by establishing a greater degree of long range order.

The field dependent magnetization ($M-H$) loops at 10 K are shown in Fig. 6. Below 130 nm, the samples do not saturate completely in fields up to 5 T. Surface spin disorder likely plays a role in preventing saturation. The magnetization at 5 T reaches only 0.21 μ_B/f.u. in the 10 nm samples. When compared with the expected spin-only moment of 3.4 μ_B/f.u. for perfectly aligned spins in $La_{0.4}Ca_{0.6}MnO_3$, this corresponds to ~6% ferromagnetic alignment. As particle size is increased, the magnetization approaches the theoretical value more closely. The 5 T magnetization in the largest particles is 2.33 μ_B/f.u., approximately 70% of full ferromagnetic alignment. The coercivity in the particles follows the opposite trend—decreasing as particle size is increased. This reduction in coercivity is favorable from a refrigeration cycle standpoint, as hysteretic losses are correspondingly reduced. Interestingly, the coercivity of the amorphous particles (>6 kOe) is several times larger than that of the other samples studied. The results of the magnetic and magnetocaloric characterization are summarized in Table 1.

To evaluate the magnetocaloric effect in the present samples, the magnetic entropy change was calculated from a series of

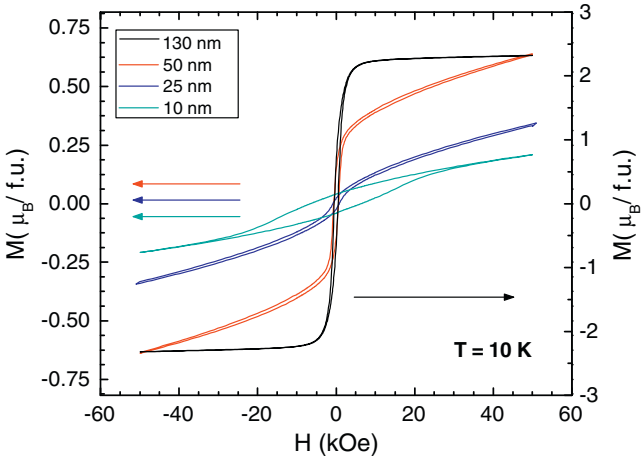

Fig. 6. Hysteresis loops measured at 10 K in the field range from −5 T to 5 T.

Table 1
The magnetic and magnetocaloric parameters of $La_{0.4}Ca_{0.6}MnO_3$ nanoparticles related to particle size.

Diameter (nm)	M (μ_B/f.u.) 10 K, 5 T	H_C (Oe) 10 K	$\lvert\Delta S_M\rvert$ (J/kg K) 5 T	RC (J/kg) 5 T
10	0.210	6402.5	0.46	8.1
25	0.344	798.8	0.13	11.0
50	0.640	596.4	0.33	46.6
130	2.33	513.3	2.81	240.7

isothermal M–H curves using the thermodynamic Maxwell relation,

$$\Delta S_M = \nu_0 \int_0^{H_{\max}} \left(\frac{\partial M}{\partial T}\right)_H dH.$$

where M is the magnetization, H is the magnetic field, and T is the temperature. Isothermal magnetization curves were taken from 0.0 to 5.0 T at 10 K temperature intervals over the region of interest in each sample. For all temperatures, magnetization increased smoothly with the applied field—a characteristic of a single-phase material. Upon integrating between the magnetization versus field curves, we observe distinct peaks in the temperature dependent entropy change (Fig. 7). By convention, we plot negative entropy change versus temperature. The maximum values of $-\Delta S_M$ for the 10 nm, 25 nm, 50 nm, and 130 nm particles were determined to be 0.46 J/kg K, 0.13 J/kg K, 0.33 J/kg K, and 2.81 J/kg K, respectively. The sharp low temperature transition in the amorphous particles gives way to smooth, broader transitions in the larger particles.

The refrigeration capacity, defined as $RC = -\Delta S_M(T,H) * \delta T_{FWHM}$, where δT_{FWHM} is the full width at half maximum of the $-\Delta S_M$ peak, is an important parameter to optimize for refrigeration applications. While the amorphous particles achieve larger $-\Delta S_M$ than the intermediate particle sizes, the narrow temperature range over which the peak extends results in a small RC value. The RC depends linearly on the applied field; over a field change of 5 T, the RC in the 130 nm particles reaches ~240 J/kg. In the range of fields that can be produced with permanent magnets (~0–2 T), these particles still produces a sizable RC of up to ~94 J/kg. Table 2 shows $-\Delta S_M$ and RC values for several representative magnetocaloric materials with curie temperatures near 250 K. Our current result for 130 nm particles compares well with those in other manganite compounds and reaches ~60% of the value of gadolinium.

A final note is that the magnetic entropy change is directly related to the first derivative of magnetization with temperature, making it a more sensitive probe of behavior near a transition temperature than magnetization or resistivity measurements alone [30]. For materials undergoing a paramagnetic to ferromagnetic phase transition, the decrease in magnetic entropy as randomly oriented spins align results in positive values for $-\Delta S_M$. On the other hand, negative values of $-\Delta S_M$ are observed in a material undergoing a ferromagnetic to antiferromagnetic transition since the configurational entropy of the spins increases as the magnetic sublattice aligns anti-parallel to the applied magnetic field [30]. The values of $-\Delta S_M$ remain positive over the entire temperature range

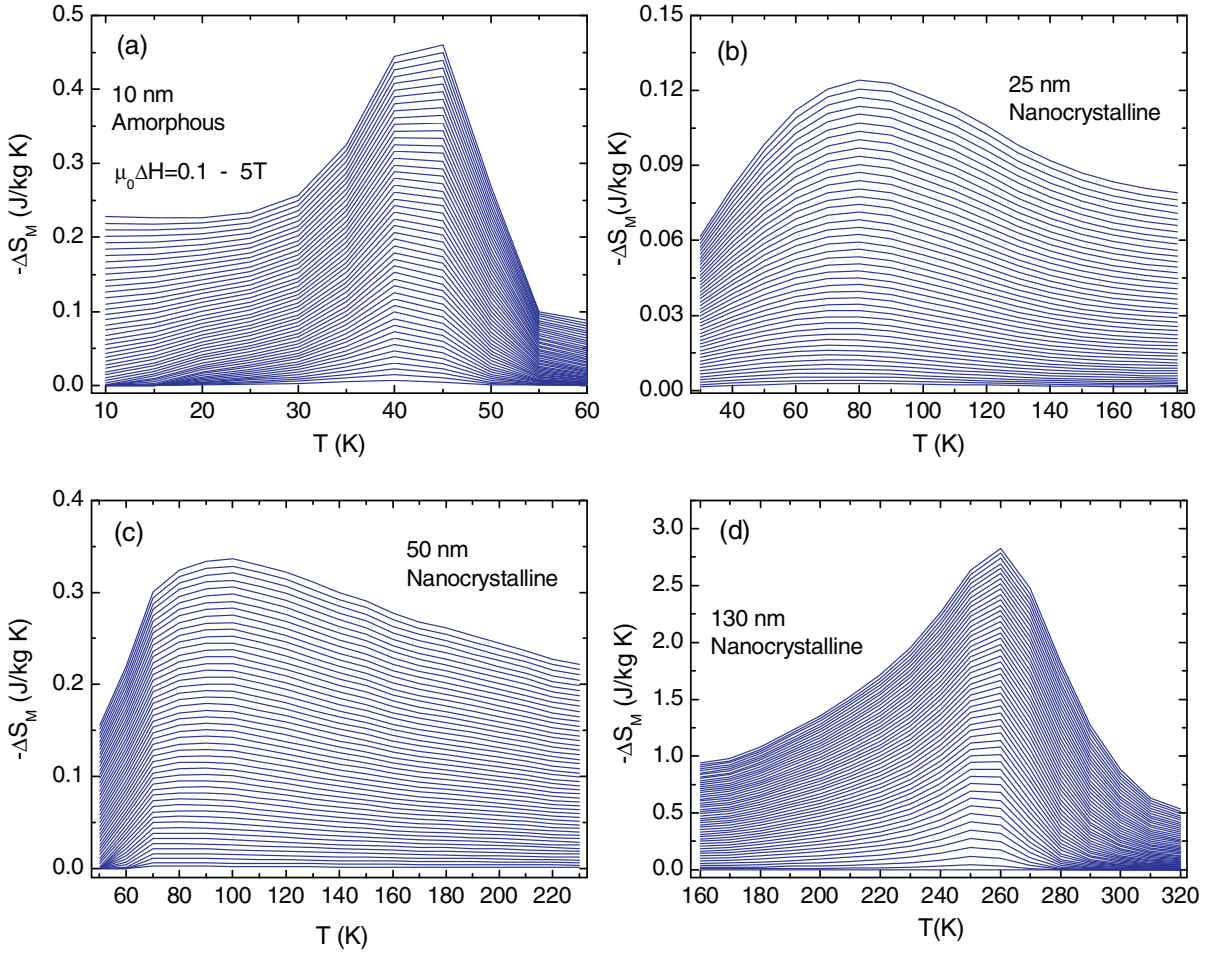

Fig. 7. Constant-field magnetic entropy change curves as a function of temperature for the (a) 10 nm amorphous, and (b) 25 nm, (c) 50 nm, and (d) 130 nm nanocrystalline particles. Measurements were carried out at field increments of 0.1 T from 0.1 to 5 T.

Table 2
The magnetocaloric parameters of typical magnetic refrigerant materials compared to 130 nm $La_{0.4}Ca_{0.6}MnO_3$.

Material	T_{peak} (K)	$\mu_0\Delta H$ (T)	$\lvert\Delta S_M\rvert$ (J/kg K)	RC (J/kg)	Reference
$La_{0.4}Ca_{0.6}MnO_3$ (130 nm)	250	5	2.81	240.7	Present
$La_{0.7}Ca_{0.3}MnO_3$ (160 nm)	270	4.5	5.02	218.4	[5]
$La_{0.7}Ca_{0.3}MnO_3$ (bulk)	235	4.5	6.99	243.1	[5]
$La_{0.67}Ca_{0.33}Mn_{0.9}V_{0.1}O_3$ (40 nm)	252	5	4.5	135	[10]
$La_{0.35}Pr_{0.275}Ca_{0.375}MnO_3$ (50 nm)	215	5	6.2	225.6	[9]
$Pr_{0.65}(Ca_{0.6}Sr_{0.4})_{0.35}MnO_3$ (78 nm)	210	7	2.5	306.6	[11]
Gd (bulk)	287.25	5	7.4	420	[6]

for all particle sizes investigated, a compelling indication that no significant CO phase is present in our samples.

4. Conclusions

In summary, we have investigated the magnetic and magnetocaloric properties of nanoparticles of $La_{0.4}Ca_{0.6}MnO_3$ prepared by a Pechini-type sol–gel method. In contrast to previous studies, no significant CO phase was observed in the system. The discrepancy is likely a consequence of oxygen deficiencies. Through the application of differing heat treatments, several sizes of particles were obtained. Increasing the particle size from 10 nm to 130 nm was found to improve crystallinity and long range ferromagnetic order while increasing magnetization and refrigerant capacity and reducing coercivity. The largest particle size exhibits a sizeable refrigerant capacity ~240 J/kg, making it a good candidate for magnetic refrigeration around 250 K.

Acknowledgments

This work was supported, in part, by the University of South Florida Internal Awards Program under Grant No. 68430 and by DOE BES Physical Behavior of Materials Program through Grant No. DE-FG02-07ER46438. MHP also acknowledges the support from the Florida Cluster for Advanced Smart Sensor Technologies (FCASST).

References

[1] V.K. Pecharsky, K.A. Gschneidner, J. Magn. Magn. Mater. 200 (1999) 44–56.
[2] M.H. Phan, S.C. Yu, J. Magn. Magn. Mater. 308 (2007) 325–340.
[3] E. Bruck, O. Tegus, X.W. Li, F.R. de Boer, K.H.J. Buschow, Physica B 327 (2003) 431–437.
[4] N.S. Bingham, M.H. Phan, H. Srikanth, M.A. Torija, C. Leighton, J. Appl. Phys. 106 (2009) 023909.
[5] W. Tang, W.J. Lu, X. Luo, B.S. Wang, X.B. Zhu, W.H. Song, Z.R. Yang, Y.P. Sun, J. Magn. Magn. Mater. 322 (2010) 2360–2368.
[6] S.P. Mathew, S.N. Kaul, Appl. Phys. Lett. 98 (2011) 172505.
[7] L.E. Hueso, P. Sande, D.R. Miguens, J. Rivas, F. Rivadulla, M.A. Lopez-Quintela, J. Appl. Phys. 91 (2002) 9943–9947.
[8] J.C. Debnath, R. Zeng, J.H. Kim, S.X. Dou, J. Magn. Magn. Mater. 323 (2011) 139–144.
[9] M.H. Phan, S. Chandra, N.S. Bingham, H. Srikanth, C.L. Zhang, S.W. Cheong, T.D. Hoang, H.D. Chinh, Appl. Phys. Lett. 97 (2010) 242506.
[10] P. Nisha, S.S. Pillai, A. Darbandi, A. Misra, K.G. Suresh, M.R. Varma, H. Hahn, J. Phys. D Appl. Phys. 43 (2010) 135001–135006.
[11] A. Biswas, T. Samanta, S. Banerjee, I. Das, J. Appl. Phys. 103 (2008) 013912.
[12] E. Rozenberg, M. Auslender, A.I. Shames, D. Mogilyansky, I. Felner, E. Sominskii, A. Gedanken, Y.M. Mukovskii, Phys. Rev. B 78 (2008) 052405.
[13] V. Markovich, I. Fita, A. Wisniewski, D. Mogilyansky, R. Puzniak, L. Titelman, C. Martin, G. Gorodetsky, Phys. Rev. B 81 (2010) 094428.
[14] K.P. Shinde, N.G. Deshpande, T. Eom, Y.P. Lee, S.H. Pawar, Mater. Sci. Eng. B 167 (2010) 202–205.
[15] A. Azarifar, P.A. Yadav, A.K. Chawla, J.P. Jog, S.I. Patil, R. Chandra, S.B. Ogale, Adv. Sci. Lett. 4 (2011) 424–430.
[16] G. Zhang, M. Liu, J. Mater. Sci. 34 (1999) 3213–3219.
[17] B.L. Cushing, V.L. Kolesnichenko, C.J. O'Connor, Chem. Rev. 104 (2004) 3893–3946.
[18] J. Lin, M. Yu, C.K. Lin, X.M. Liu, J. Phys. Chem. C 111 (2007) 5835–5845.
[19] C.L. Lu, S. Dong, K.F. Wang, F. Gao, P.L. Li, L.Y. Lv, J.M. Liu, Appl. Phys. Lett. 91 (2007) 032502.
[20] L. Liu, J.J. Zheng, Z.C. Xia, S.L. Yuan, Z.M. Tian, Solid State Commun. 150 (2010) 2322–2324.
[21] T. Sarkar, A.K. Raychaudhuri, A.K. Bera, S.M. Yusuf, New J. Phys. 12 (2010) 123026.
[22] S. Dong, R. Yu, S. Yunoki, J.M. Liu, E. Dagotto, Phys. Rev. B 78 (2008) 201102.
[23] S.V. Trukhanov, N.V. Kasper, I.O. Troyanchuk, M. Tovar, H. Szymczak, K. Barner, J. Solid State Chem. 169 (2002) 85–95.
[24] K.F. Wang, Y. Wang, L.F. Wang, S. Dong, D. Li, Z.D. Zhang, H. Yu, Q.C. Li, J.M. Liu, Phys. Rev. B 73 (2006) 134411.
[25] C.L. Lu, K.F. Wang, S. Dong, J.G. Wan, J.M. Liu, Z.F. Ren, J. Appl. Phys. 103 (2008), 07F714.
[26] V.N. Krivoruchko, M.A. Marchenko, Y. Melikhov, Phys. Rev. B 82 (2010) 064419.
[27] S.M. Zhou, S.Y. Zhao, Y.Q. Guo, J.Y. Zhao, L. Shi, J. Appl. Phys. 107 (2010) 033906.
[28] W.J. Jiang, X.Z. Zhou, G. Williams, Y. Mukovskii, R. Privezentsev, J. Appl. Phys. 107 (2010), 09D701.
[29] S.K. Banerjee, Phys. Lett. 12 (1964) 16–17.
[30] M.H. Phan, M.B. Morales, N.S. Bingham, H. Srikanth, C.L. Zhang, S.W. Cheong, Phys. Rev. B 81 (2010) 094413.